Supporting Information

A Comparative Study on Surface-engineered Nanoceria Using a Catechol Copolymer Design: Colloidal Stability vs. Antioxidant Activity

Milad Ghorbani[1,2], Francesca Ercole[1], Katayoun Nazemi[1], Nicole M. Warne[1], John F. Quinn[1,3*], Kristian Kempe[1,2*]

[1] Drug Delivery, Disposition and Dynamics, Monash Institute of Pharmaceutical Sciences, Monash University, Parkville, Victoria 3052, Australia

[2] Materials Science and Engineering, Monash University, Clayton, Victoria 3800, Australia

[3] Department of Chemical Engineering, Faculty of Engineering, Monash University, Clayton, Victoria 3800, Australia

* Corresponding authors

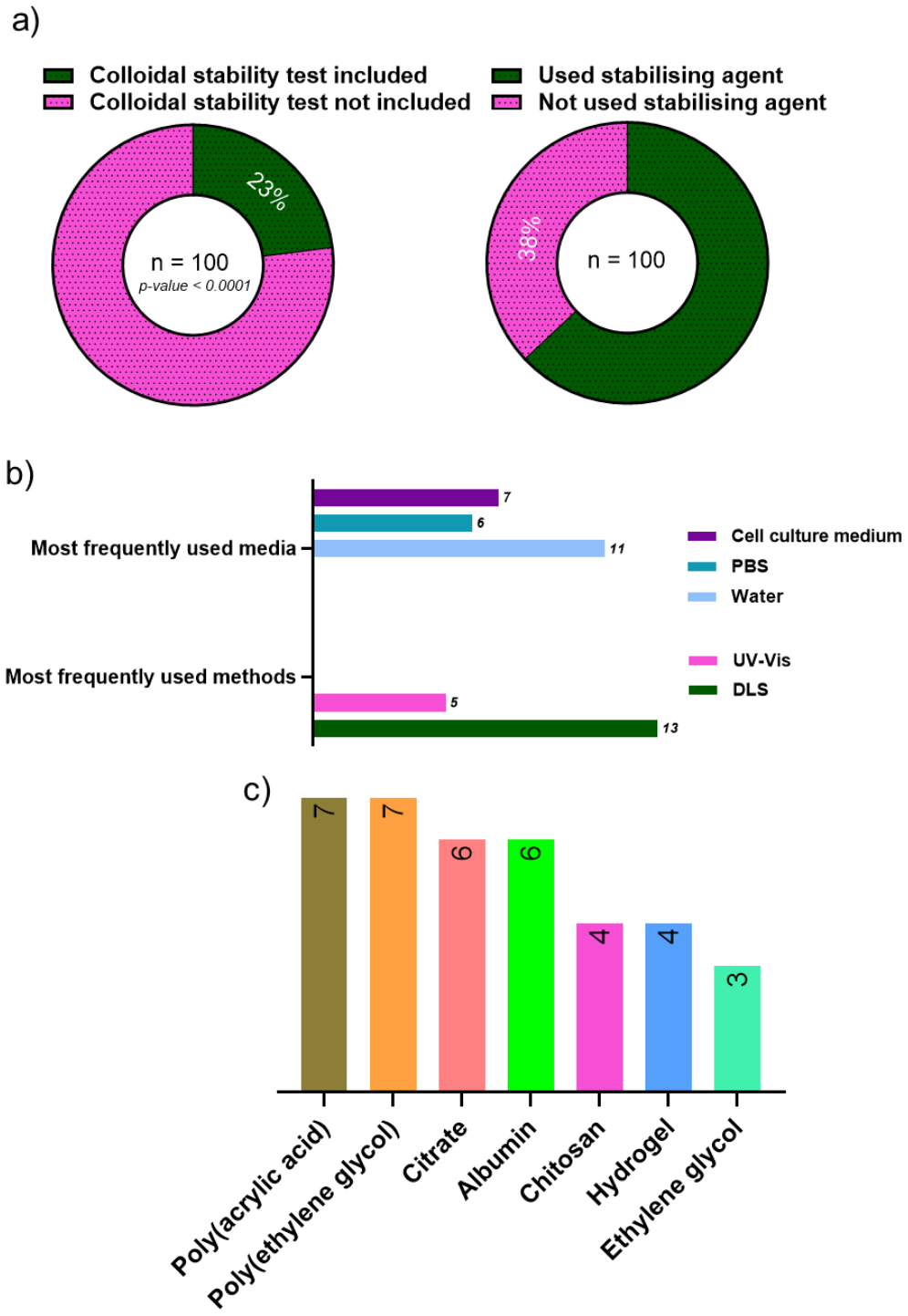

Fig. S1 A sample population of 100 papers (out of 235 papers; confidence interval 99%) published in Q1 journals since 2016 was randomly selected via searching Scopus library (keywords: nanoceria, cerium oxide, antioxidant): a) Colloidal stability analysis was found almost a missing factor in studies done on antioxidant activity of nanoceria (NC), as there was a significant difference between two groups (chi-squared test, $P < 0.0001$, expected value for each group 50%). b) The most frequently used media and methods to study colloidal stability. c) The most frequently used stabilising agents. In case of "hydrogel", NC are embedded into the hydrogel structure.

Table S1. A summary of the results reported in 23 publications (out of 100 selected) addressing colloidal stability of NC since 2015.

Stabilising agent/system	Stability test method (media)	Stability test time period	Stability test outcome	Effect of colloidal stability on antioxidant activity	Ref.
Acetic acid	Apparent precipitation (water)	Several months (details N/A)	No apparent precipitation	N/A	(1)
1,2-distearoyl-sn-glycero-3-phosphoethanolamine-N-[amino(polyethylene glycol)-2000-triphenylphosphonium (DSPE-PEG-TPP)	DLS (PBS 1X, DMEM with FBS 10%, and human blood plasma)	One month	No significant change in size	Reduced CAT- and SOD-like activities	(2)
Ethylene glycol or (3-aminopropyl)triethoxysilane (APTES) or Pluronic F127 or 6-{2-[2-(2-Methoxy-ethoxy)-ethoxy]-ethoxy-hexyl)triethoxysilane (MEEETES)	UV-Vis (water pH 7.4)	Two weeks	Around 90%, 40%, and 25% precipitation for Pluronic F127, ethylene glycol, and MEEETES coated NC, respectively. Very low stability for APTES coated NC.	No direct correlation between colloidal stability and OH• scavenging activity	(3)
Loaded in liposomes	DLS (water)	One month	<15% variation in size	N/A	(4)
Glycol chitosan polymer matrix	Apparent change in colour and structure (water)	One year	No change in colour, no degradation	Significant increase in antioxidant capacity	(5)

Triethylene glycol	DLS (water)	One month	N/A	N/A	(6)
Oligochitosan coated nanoceria loaded in injectable alginate-gelatin hydrogels	DLS (water)	N/A	N/A	N/A	(7)
Loaded in nanostructured lipid carriers	DLS (PBS 1X, DMEM with and without FBS 10%)	70 min	No aggregation and/or significant fluctuation in size	No significant change in OH• scavenging activity	(8)
Polyethylene glycol (PEG 600) or glycine	UV-Vis (acetate buffer pH 4.4, phosphate buffer pH 7.0, or bicarbonate buffer pH 9.2)	N/A	No significant change in nature and position of the peaks in each medium	N/A	(9)
Ethylene glycol	UV-Vis (water)	One week	No significant change in NC concentration in supernatant	N/A	(10)
Branched polyethylenimine (PEI 1800)	Antioxidant activity against 1,1-diphenyl-2-picryhydrazyl (DPPH) (Methanol)	Two weeks	No significant change in antioxidant activity	N/A	(11)
Rat serum albumin	UV-Vis (DMEM with FBS)	One week	N/A	N/A	(12)

Dextran or poly(acrylic acid) or methoxyacetic acid	DLS (water, water with BSA, and DMEM with and without FBS)	N/A	No significant agglomeration in water and DMEM with and without FBS for poly(acrylic acid) coated NC media, while noticeable agglomeration in water with BSA medium. No significant agglomeration in water DMEM without FBS media for dextran coated NC, while noticeable agglomeration in water with BSA and DMEM with FBS media. Significant increase in size for methoxyacetic acid coated NC in either medium.	Significant increase in CAT-like activity in water medium for all samples, while no direct correlation for SOD- and CAT-like activity in DMEM with and without FBS media	(13)
Alkoxy-silyl-fulleropyrrolidine	Apparent precipitation (water)	Three months	No apparent precipitation	N/A	(14)
Montmorillonite	TEM, XRD, ICP, and antioxidant activity (simulated gastric fluid pH 1.2-1.5)	Four hours	Retained structural integrity	Slight increase in SOD-like activity, while slight decrease in CAT-like and OH• scavenging activities	(15)

Fetal bovine serum (FBS)	DLS at normal gravity and microgravity 20°/s (water, water with 10% FBS, and complete cell culture medium: CO_2-independent medium, Gibco 18045088, added with 10% FBS, 100 U/mL penicillin-100 μg/mL streptomycin, Gibco 15140122)	Two weeks	No significant change in size	N/A	(16)
Trisodium citrate coated nanoceria embedded in chitosan matrix	DLS (0.1 M trisodium citrate solution for trisodium citrate coated nanoceria)	Six days for trisodium citrate coated nanoceria	No significant change in size and surface charge	N/A	(17)
Albumin	DLS (PBS)	25 days	No significant change in size	N/A	(18)
Polyethylene glycol (PEG 600)	UV-Vis (water and PBS)	90 min	No significant precipitation	Slight increase in radical scavenging activity	(19)
SiO_2 shell or tetradecyltrimethylammonium bromide (TTAB)	DLS (acidic solution pH 2, radical solution 2 wt% H_2O_2 + 3 ppm Fe(II))	Three days	No significant increase in size for SiO_2 shell stabilised NC in both solutions, while >10-fold and >100-fold increase in size for TTAB	N/A	(20)

			stabilised NC in radical and acidic solutions, respectively.		
Albumin	DLS (N/A)	Four days	No significant change in size	N/A	(21)
Polyethylene glycol (PEG 2000)	DLS (histidine-tryptophan-ketoglutarate (HTK) solution)	One week	No significant change in size	N/A	(22)
Albumin	DLS (water, PBS, normal saline, DMEM)	Two days	No significant change in size	N/A	(23)

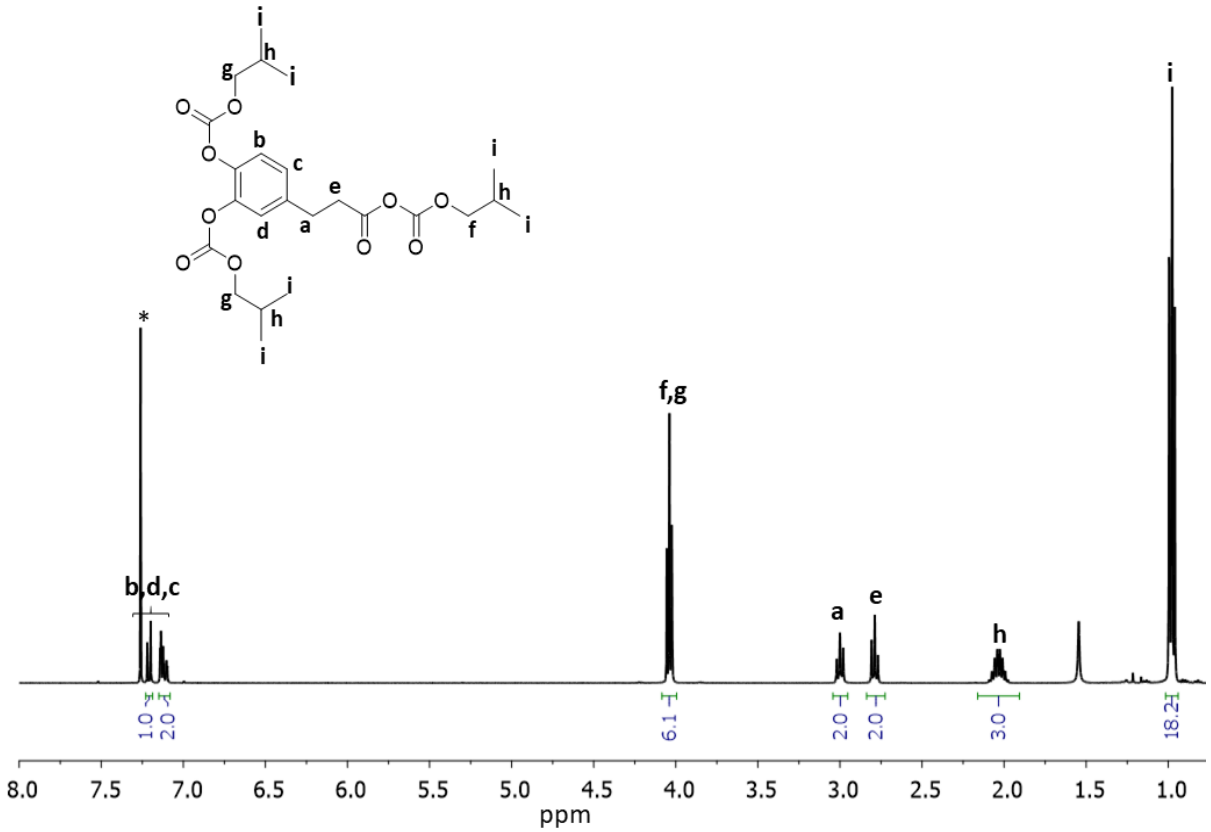

Fig. S2 ^{1}H NMR (400 MHz, $CDCl_3$) spectrum of iBocHCAF. *Residual NMR solvent peak.

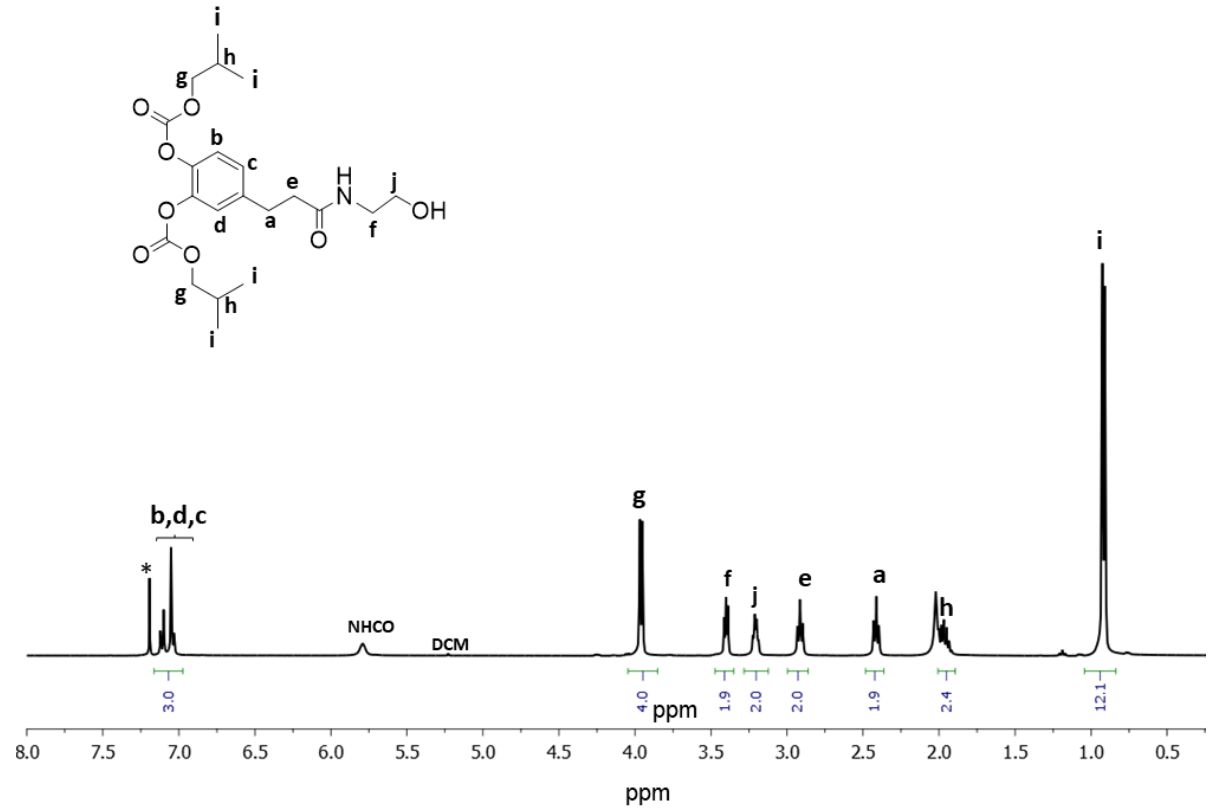

Fig. S3 ^{1}H NMR (400 MHz, $CDCl_3$) spectrum of iBocDHCA-HEA. *Residual NMR solvent peak.

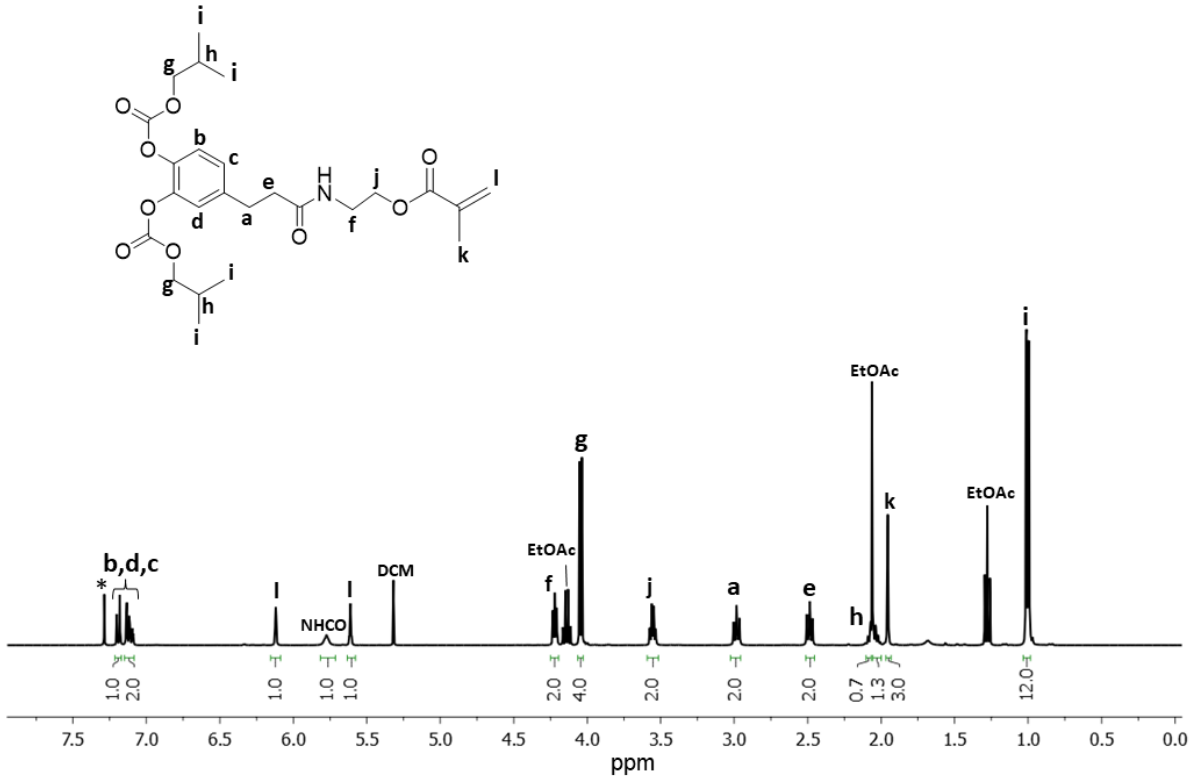

Fig. S4 ^{1}H NMR (400 MHz, $CDCl_3$) spectrum of 2-((3-(3,4-bis((isobutoxycarbonyl) oxy)phenyl)propanoyl)oxy)ethyl methacrylate (**prCAT**). *Residual NMR solvent peak.

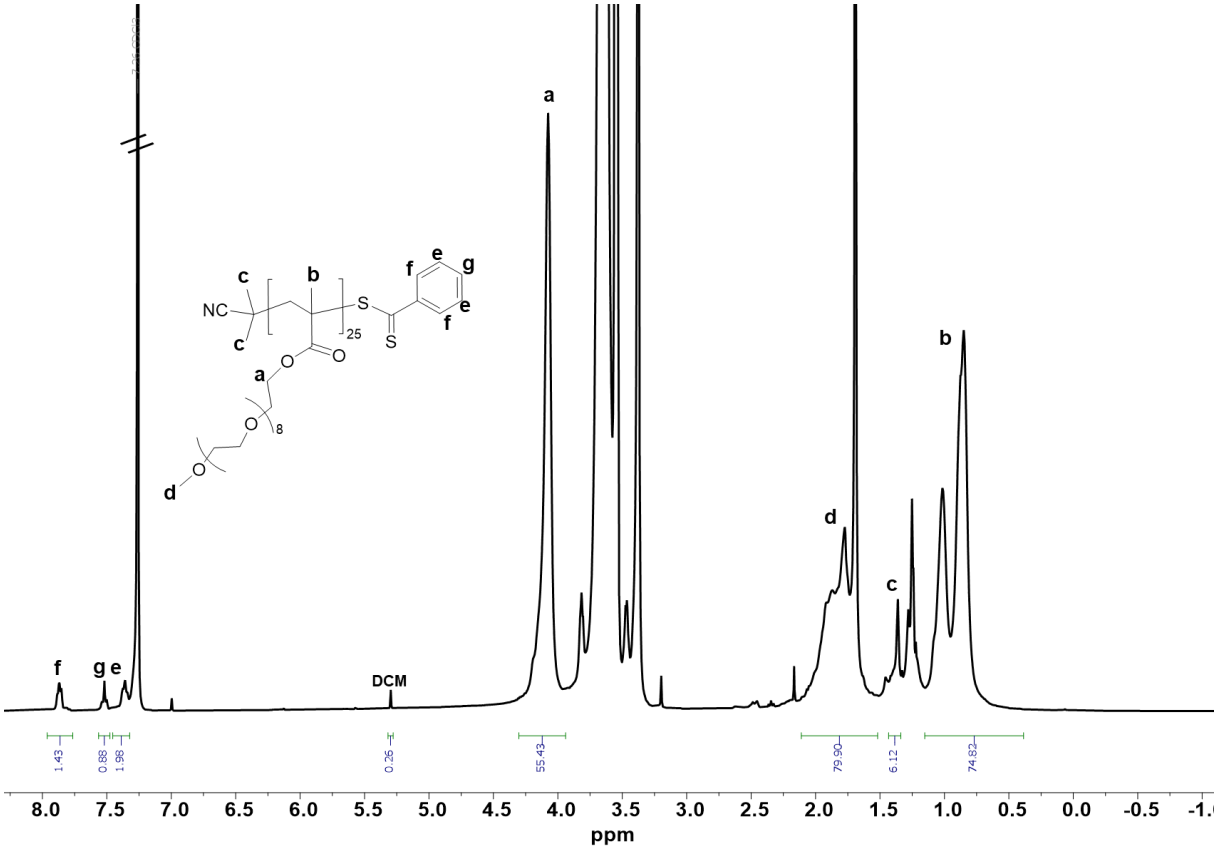

Fig. S5 ^{1}H NMR (400 MHz, $CDCl_3$) spectrum of $P(OEGMA)_{25}$.

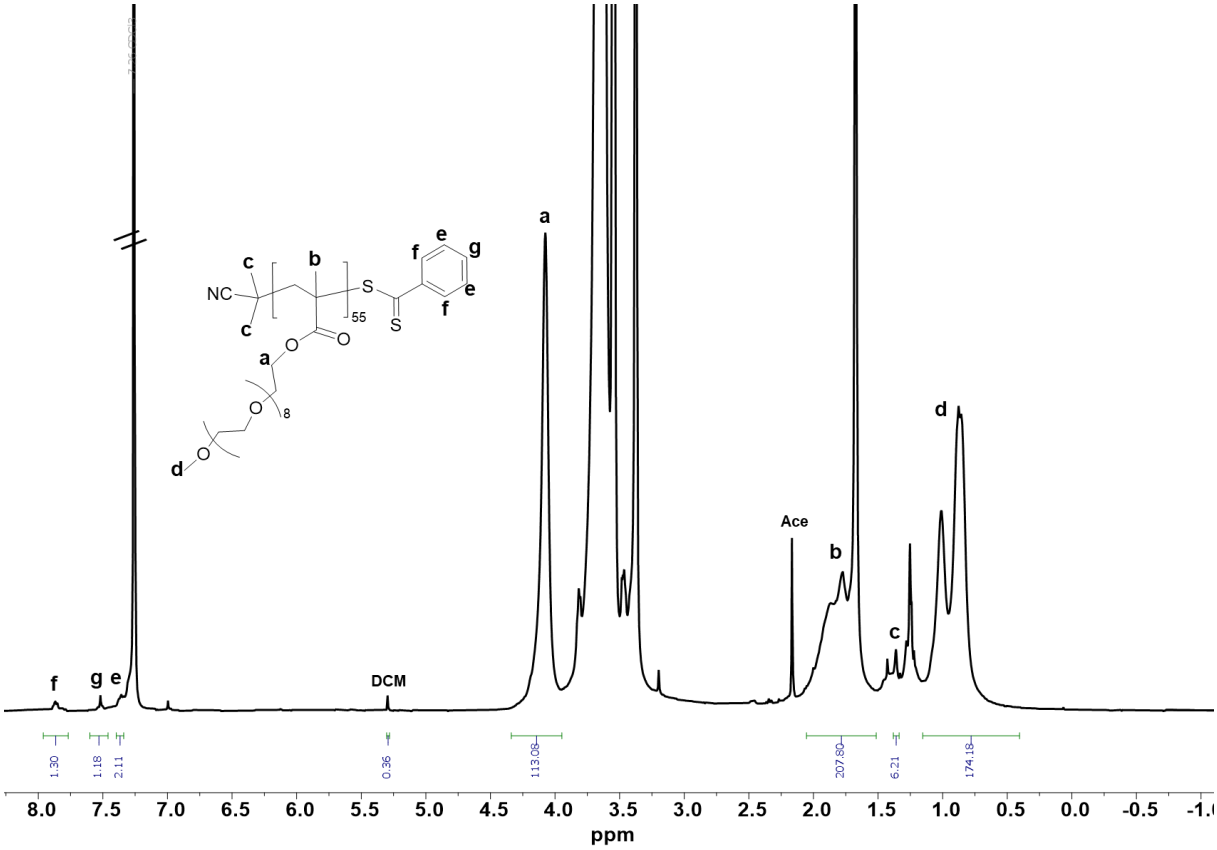

Fig. S6 ^{1}H NMR (400 MHz, $CDCl_3$) spectrum of $P(OEGMA)_{55}$.

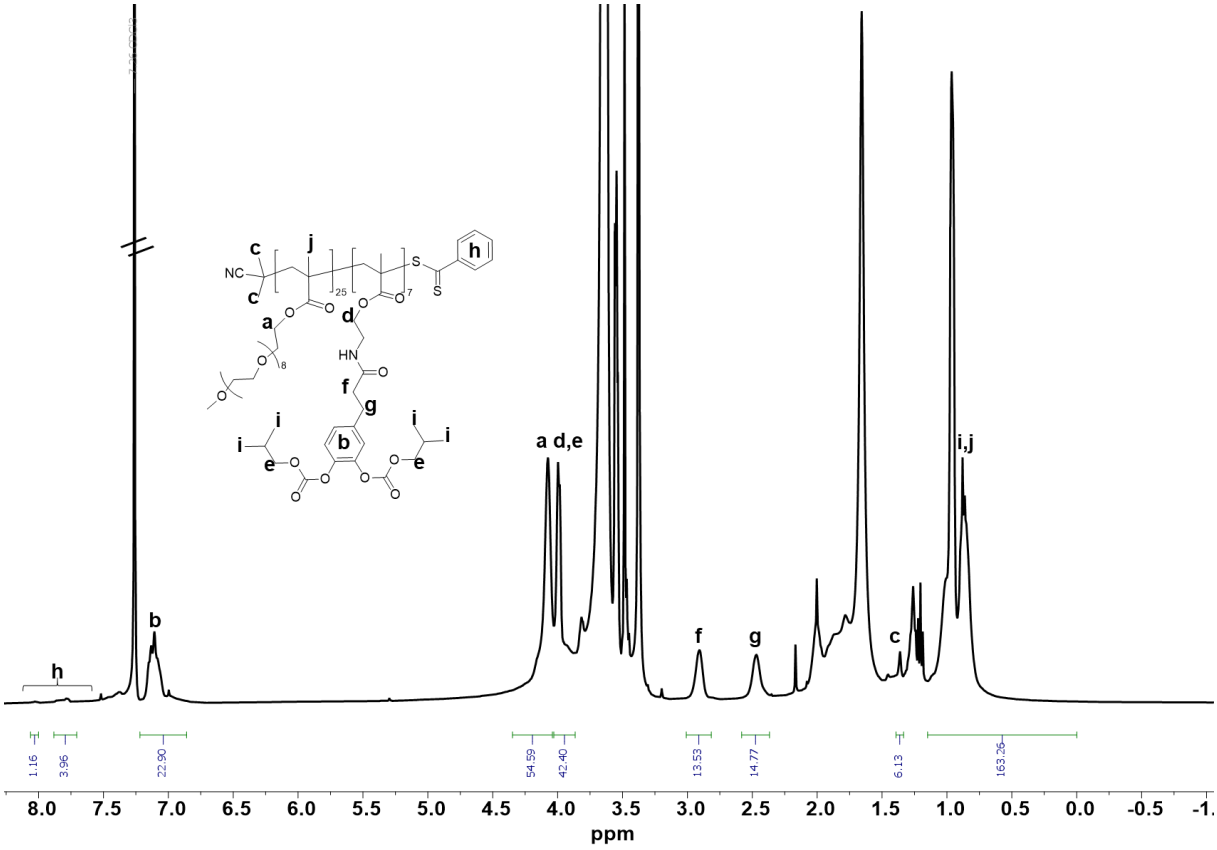

Fig. S7 ^{1}H NMR (400 MHz, $CDCl_3$) spectrum of $P(OEGMA)_{25}$-*b*-$P(prCAT)_7$-S-(C=S)-Ph.

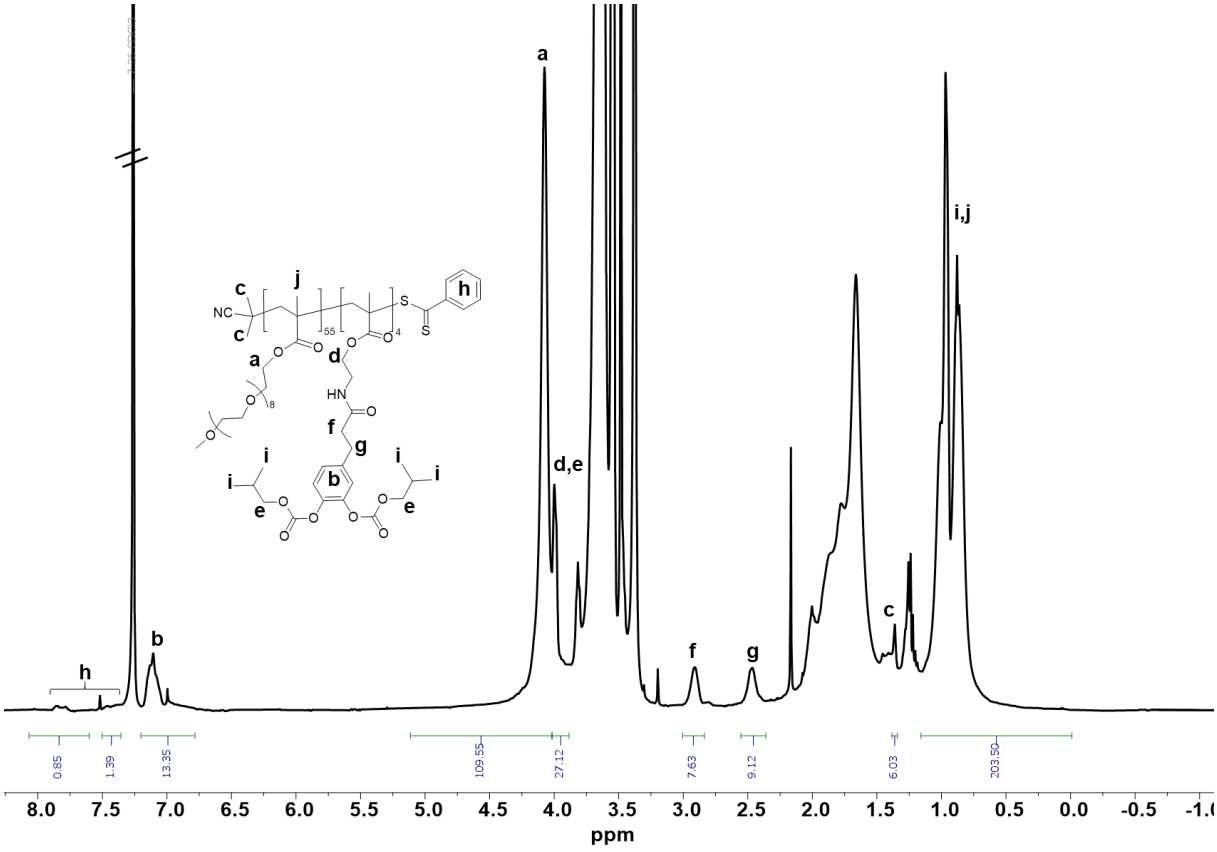

Fig. S8 ^{1}H NMR (400 MHz, $CDCl_3$) spectrum of $P(OEGMA)_{55}$-*b*-$P(prCAT)_4$-S-(C=S)-Ph.

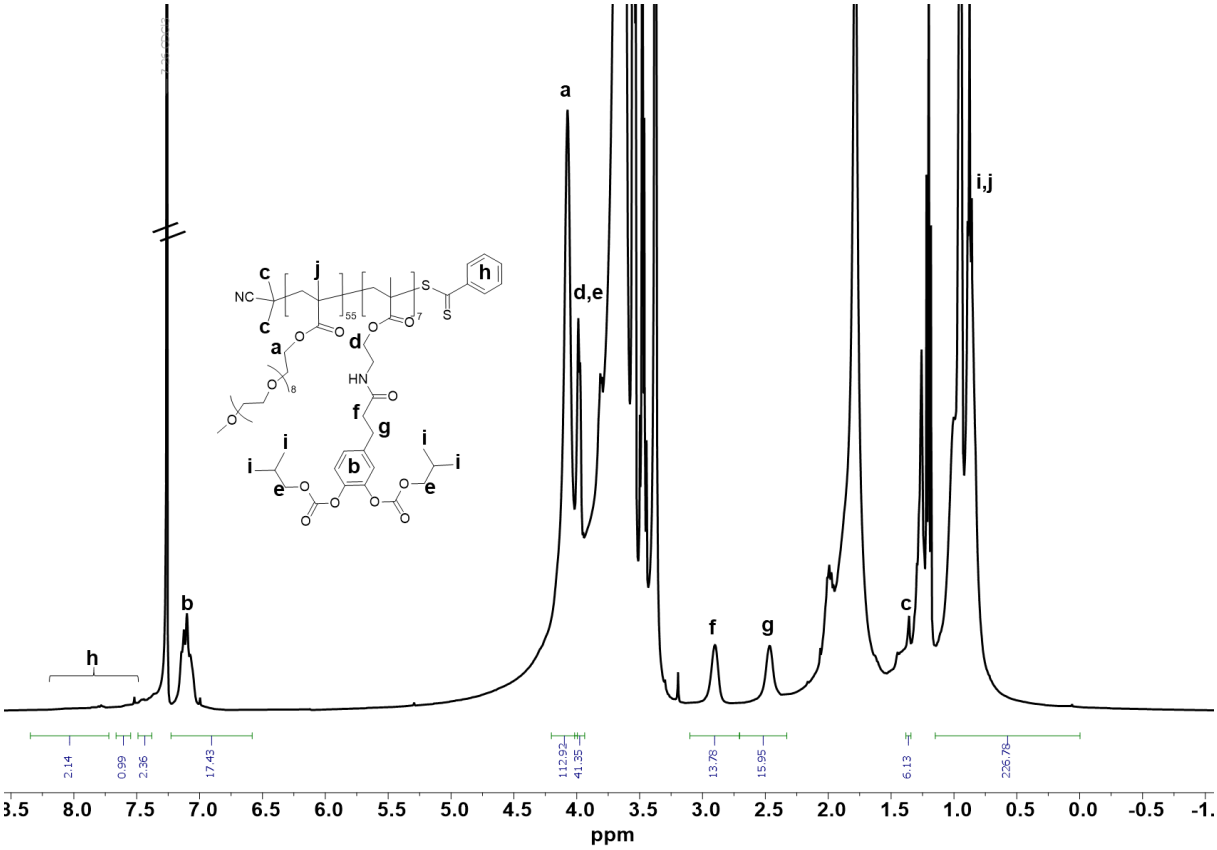

Fig. S9 ^{1}H NMR (400 MHz, $CDCl_3$) spectrum of $P(OEGMA)_{55}$-*b*-$P(prCAT)_7$-S-(C=S)-Ph.

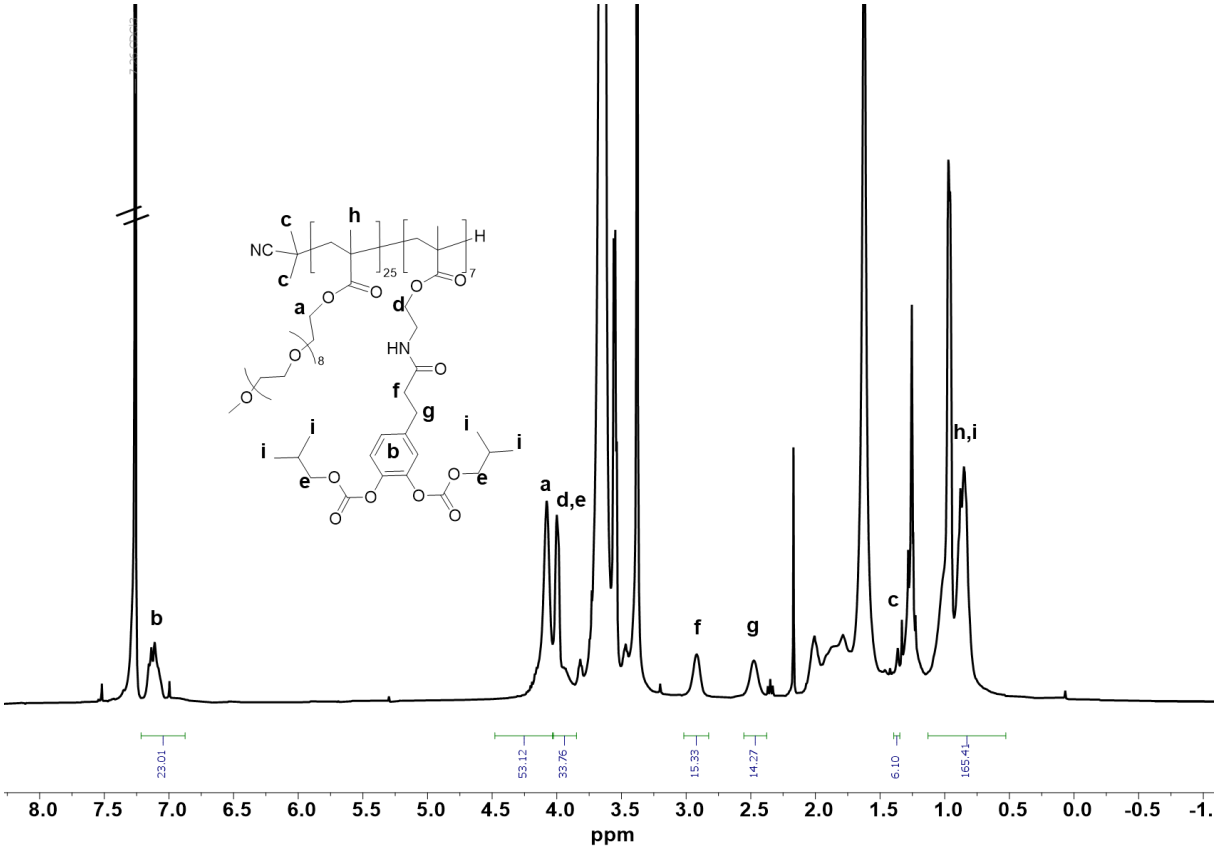

Fig. S10 ^{1}H NMR (400 MHz, $CDCl_3$) spectrum of $P(OEGMA)_{25}$-*b*-$P(prCAT)_7$.

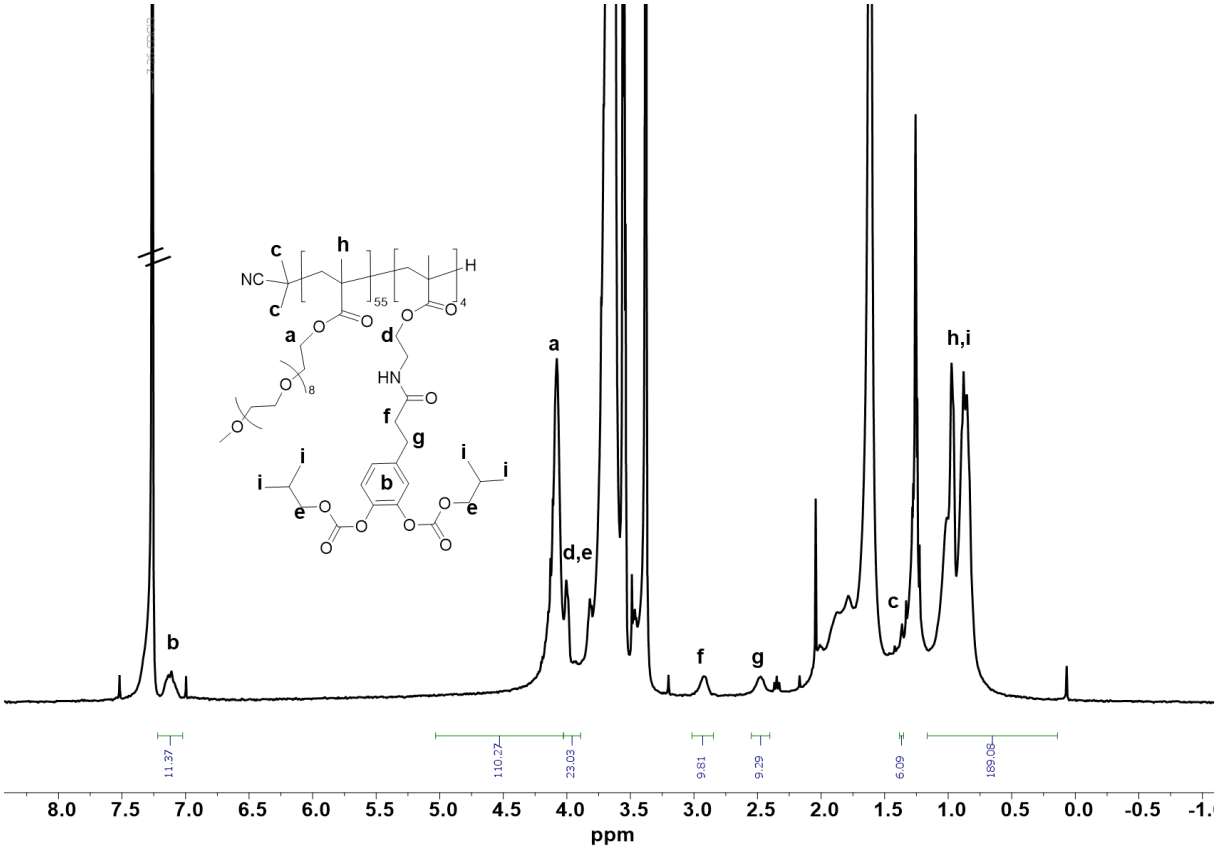

Fig. S11 ^{1}H NMR (400 MHz, $CDCl_3$) spectrum of P(OEGMA)$_{55}$-*b*-P(prCAT)$_4$.

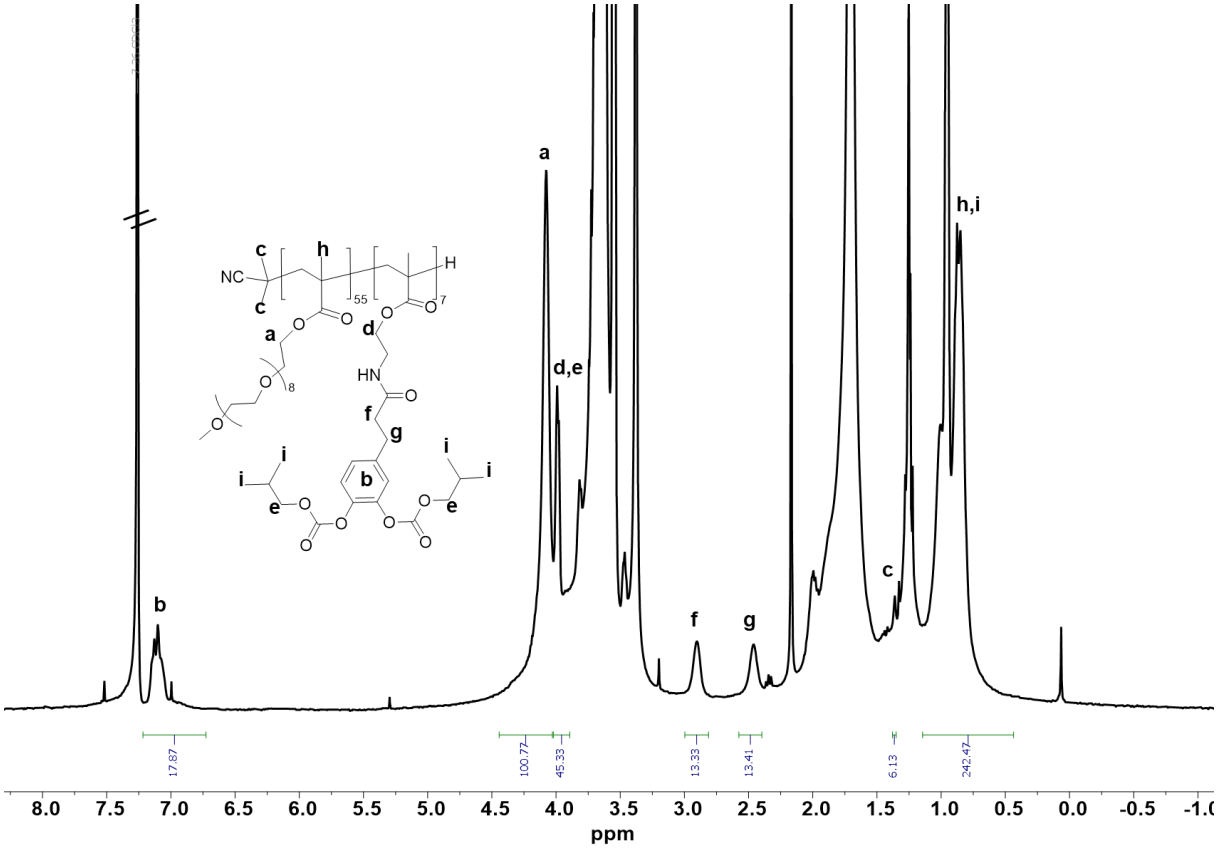

Fig. S12 ^{1}H NMR (400 MHz, $CDCl_3$) spectrum of $P(OEGMA)_{55}$-*b*-$P(prCAT)_7$.

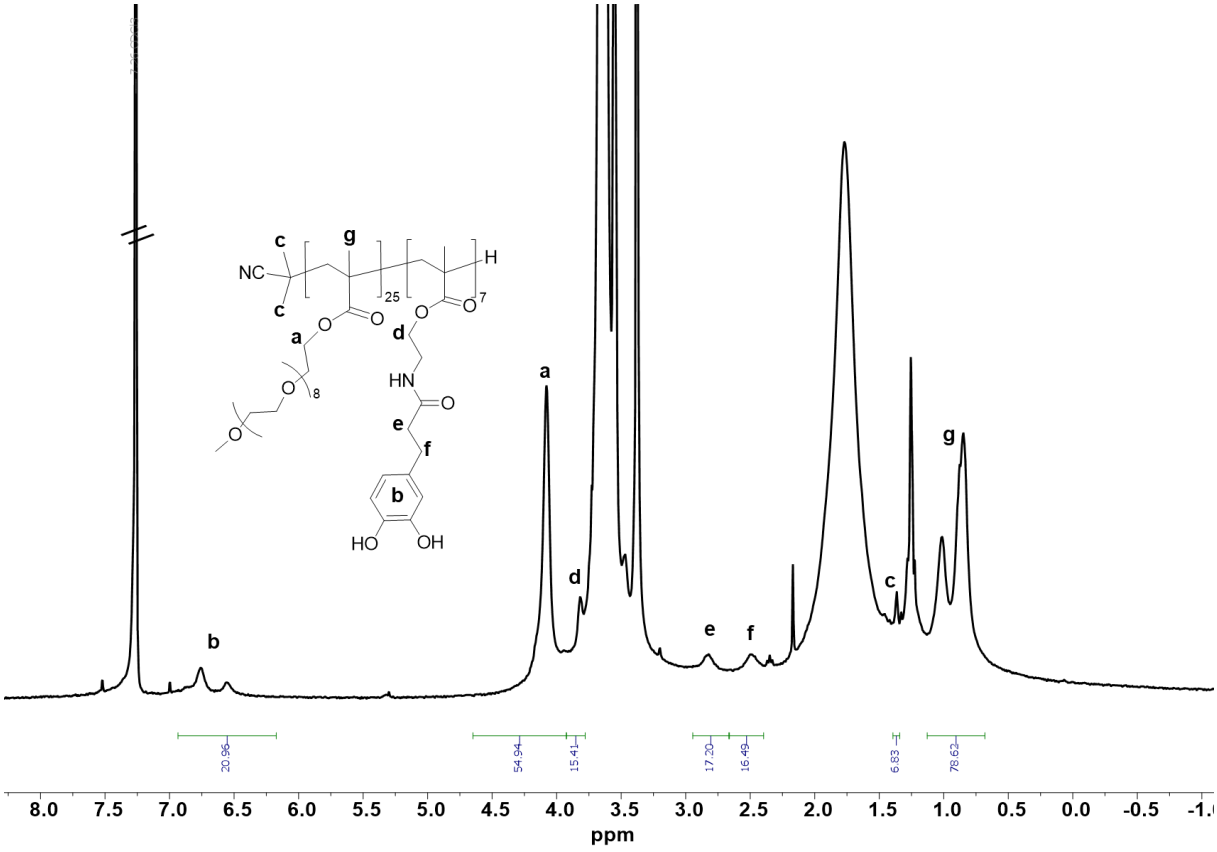

Fig. S13 ^{1}H NMR (400 MHz, $CDCl_3$) spectrum of $P(OEGMA)_{25}$-*b*-$P(CAT)_7$.

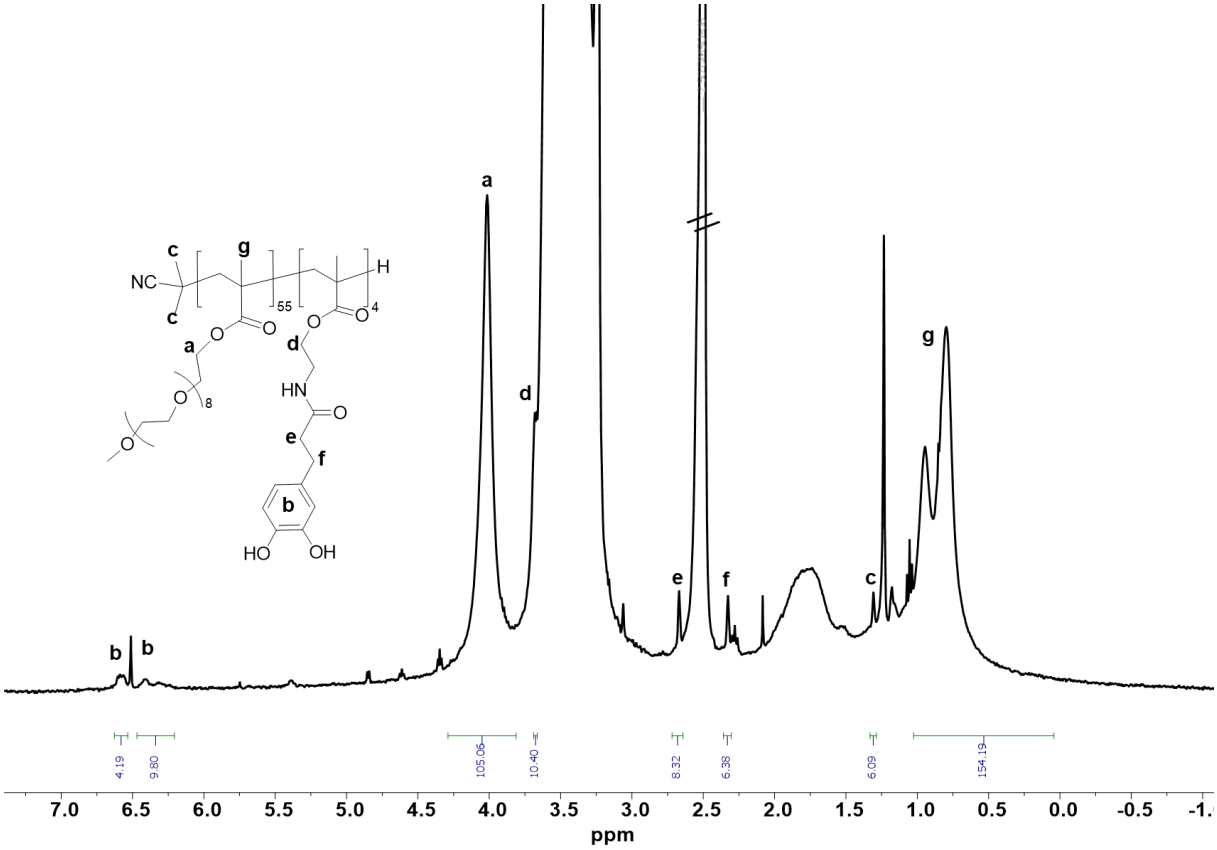

Fig. S14 ^{1}H NMR (400 MHz, DMSO-d_6) spectrum of P(OEGMA)$_{55}$-*b*-P(CAT)$_4$.

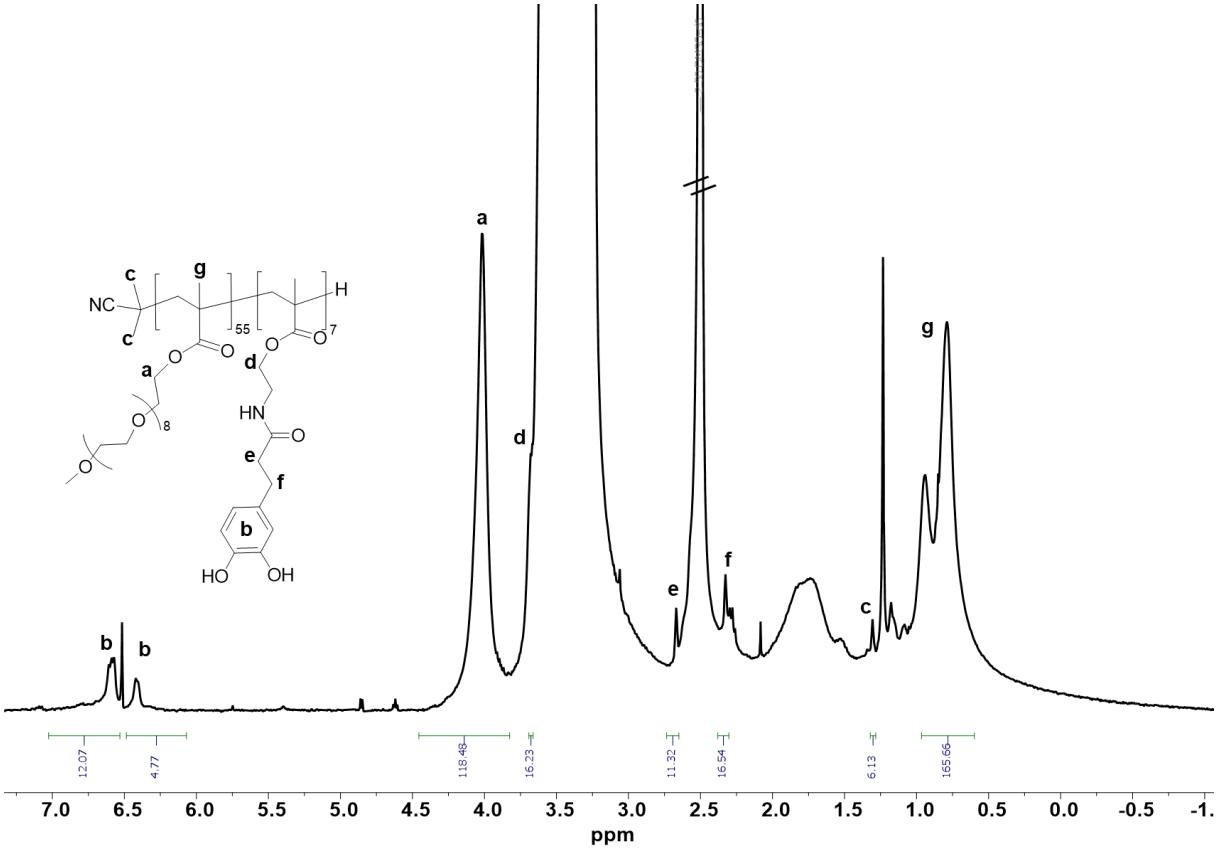

Fig. S15 ^{1}H NMR (400 MHz, DMSO-d_6) spectrum of P(OEGMA)$_{55}$-*b*-P(CAT)$_7$.

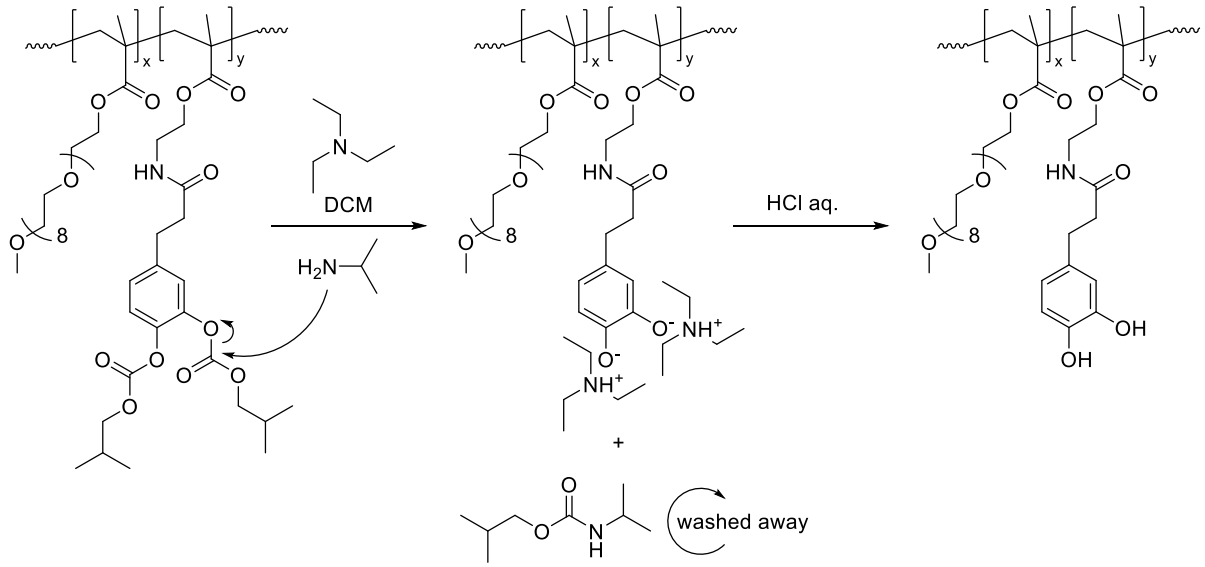

Scheme S1. Schematic representation of carbonate deprotection reaction using isopropyl amine to generate P(OEGMA)$_x$-*b*-P(CAT)$_y$.

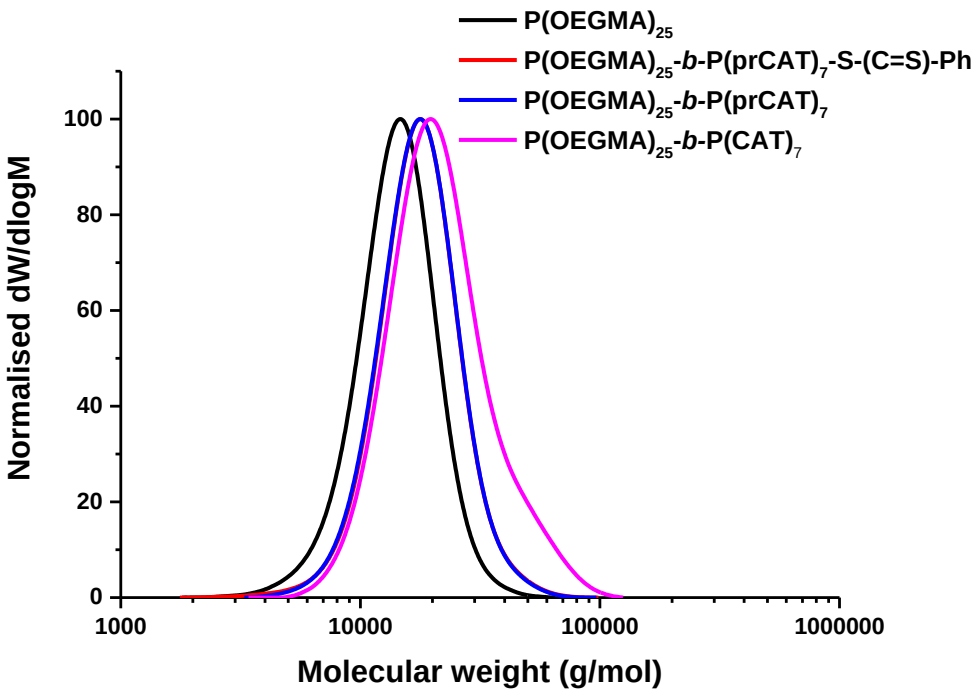

Fig. S16 SEC (DMAc) molecular weight distribution graphs of the final products at each step towards synthesis of P(OEGMA)$_{25}$-*b*-P(CAT)$_{7}$.

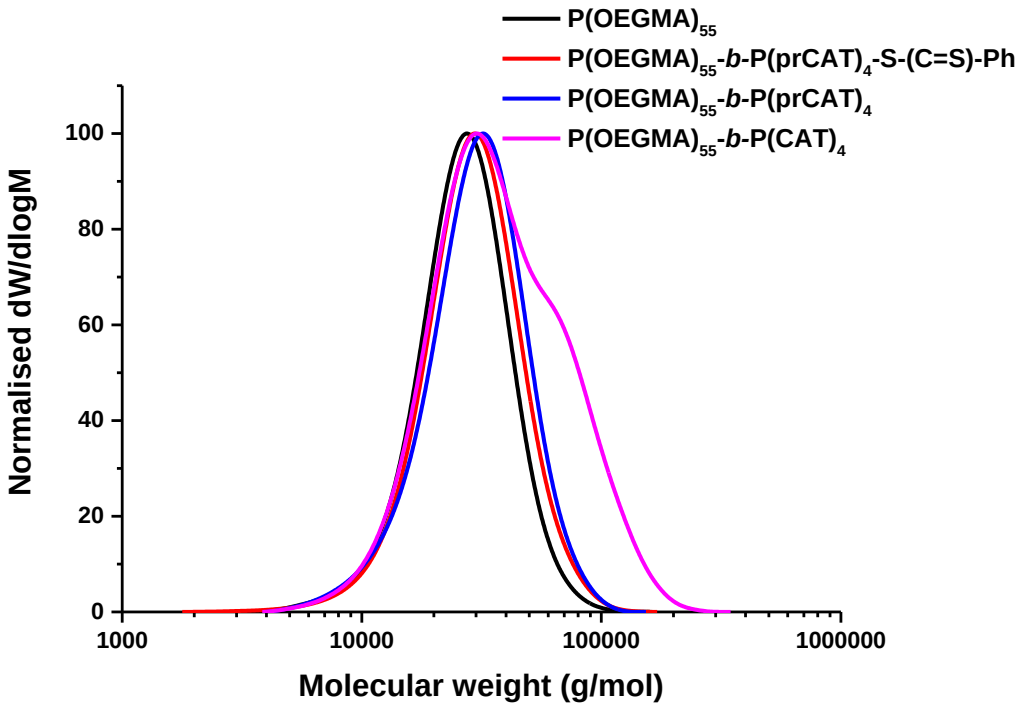

Fig. S17 SEC (DMAc) molecular weight distribution graphs of the final products at each step towards synthesis of P(OEGMA)$_{55}$-*b*-P(CAT)$_{4}$.

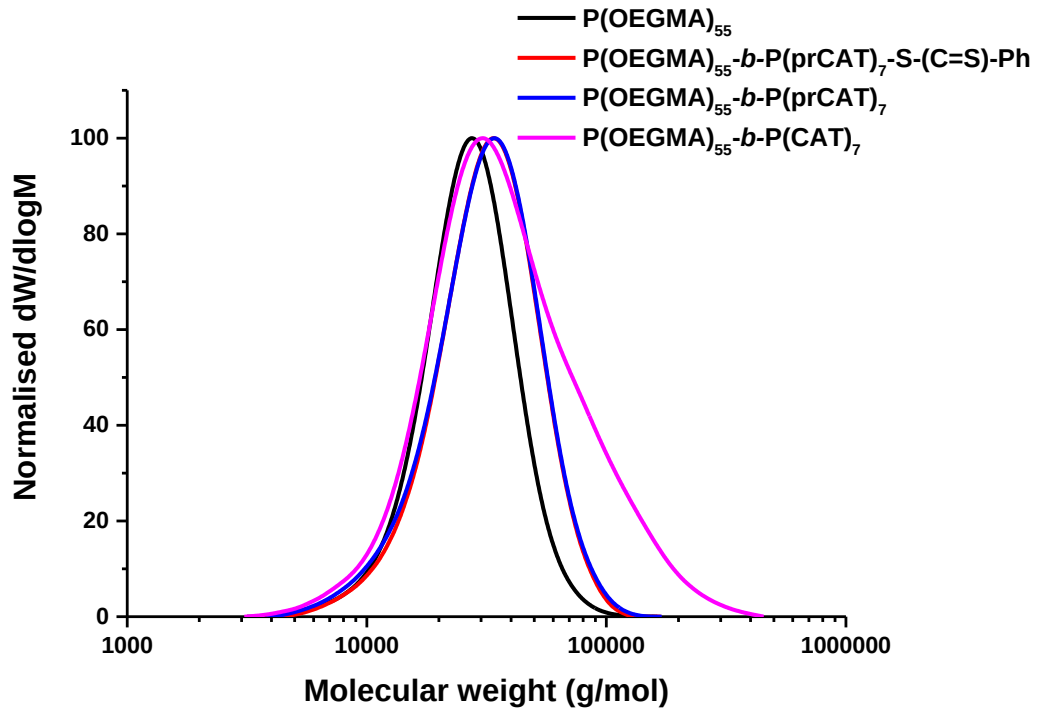

Fig. S18 SEC (DMAc) molecular weight distribution graphs of the final products at each step towards synthesis of P(OEGMA)$_{55}$-*b*-P(CAT)$_7$.

Table S2. RAFT end-group removal from P(OEGMA)$_x$-*b*-P(prCAT)$_y$-S-(C=S)-Ph (**2a,2b,2c**).

Before RAFT end group removal		**After RAFT end group removal**			
^{1}H NMR Composition of precursor polymer	**SEC UV Detector MAX intensity (310 nm)/RI detector MAX intensity**	**^{1}H NMR Composition**	**M_n (SEC) ($\times 10^3$ g/mol)**	**Đ**	**SEC UV Detector MAX intensity (310 nm)/RI detector MAX intensity**
P(OEGMA)$_{25}$-*b*-P(prCAT)$_7$-S-(C=S)-Ph (2a)	0.60	**P(OEGMA)$_{25}$-*b*-P(prCAT)$_7$ (3a)**	16.01	1.17	0.04
P(OEGMA)$_{55}$-*b*-P(prCAT)$_4$-S-(C=S)-Ph (2b)	0.88	**P(OEGMA)$_{55}$-*b*-P(prCAT)$_4$ (3b)**	26.10	1.27	0.11
P(OEGMA)$_{55}$-*b*-P(prCAT)$_7$-S-(C=S)-Ph (2c)	0.85	**P(OEGMA)$_{55}$-*b*-P(prCAT)$_7$ (3c)**	26.78	1.31	0.11

Table S3. The summary of synthesis and characterisation data for polymerisation of $P(OEGMA)_x$-*b*-$P(CAT)_y$ in four steps.

^{1}H NMR Composition	**Molar ratios**	**Conversion (%)**	**M_n (SEC) ($\times 10^3$ g/mol)**	**M_n (NMR) ($\times 10^3$ g/mol)**	**Đ**
$P(OEGMA)_{25}$ (1a)	$[CPBDT]_0$:$[OEGMA]_0$:$[AIBN]_0$ = 1:50:0.15	50	12.87	12.63	1.16
$P(OEGMA)_{55}$ (1b)	$[CPBDT]_0$:$[OEGMA]_0$:$[AIBN]_0$ = 1:100:0.15	55	23.46	27.53	1.23
$P(OEGMA)_{25}$-*b*-$P(prCAT)_7$-S-(C=S)-Ph (2a)	$[P(OEGMA)_{25}]_0$:$[prCAT]_0$:$[AIBN]_0$ = 1:15:0.15	50	15.86	16.09	1.18
$P(OEGMA)_{55}$-*b*-$P(prCAT)_4$-S-(C=S)-Ph (2b)	$[P(OEGMA)_{55}]_0$:$[prCAT]_0$:$[AIBN]_0$ = 1:15:0.20	30	25.18	29.50	1.27
$P(OEGMA)_{55}$-*b*-$P(prCAT)_7$-S-(C=S)-Ph (2c)	$[P(OEGMA)_{55}]_0$:$[prCAT]_0$:$[AIBN]_0$ = 1:15:0.20	50	27.51	30.98	1.28
$P(OEGMA)_{25}$-*b*-$P(prCAT)_7$ (3a)	$[P(OEGMA)_{25}$-*b*-$P(prCAT)_7$-S-(C=S)-Ph$]_0$:$[EPHP]_0$:$[ACHN]_0$ = 1:10:0.40	93	16.01	15.93	1.17
$P(OEGMA)_{55}$-*b*-$P(prCAT)_4$ (3b)	$[P(OEGMA)_{55}$-*b*-$P(prCAT)_4$-S-(C=S)-Ph$]_0$:$[EPHP]_0$:$[ACHN]_0$ = 1:10:0.45	88	26.10	29.35	1.27
$P(OEGMA)_{55}$-*b*-$P(prCAT)_7$ (3c)	$[P(OEGMA)_{55}$-*b*-$P(prCAT)_7$-S-(C=S)-Ph$]_0$:$[EPHP]_0$:$[ACHN]_0$ = 1:10:0.45	87	26.78	30.83	1.31
$P(OEGMA)_{25}$-*b*-$P(CAT)_7$ (4a)	$[P(OEGMA)_{25}$-*b*-$P(prCAT)_7]_0$:$[TEA]_0$:$[IPAM]_0$ = 1:28:140	100	19.00	14.53	1.26
$P(OEGMA)_{55}$-*b*-$P(CAT)_4$ (4b)	$[P(OEGMA)_{55}$-*b*-$P(prCAT)_4]_0$:$[TEA]_0$:$[IPAM]_0$ = 1:16:80	100	30.12	28.55	1.49
$P(OEGMA)_{55}$-*b*-$P(CAT)_7$ (4c)	$[P(OEGMA)_{55}$-*b*-$P(prCAT)_7]_0$:$[TEA]_0$:$[IPAM]_0$ = 1:28:140	100	28.89	29.43	1.68

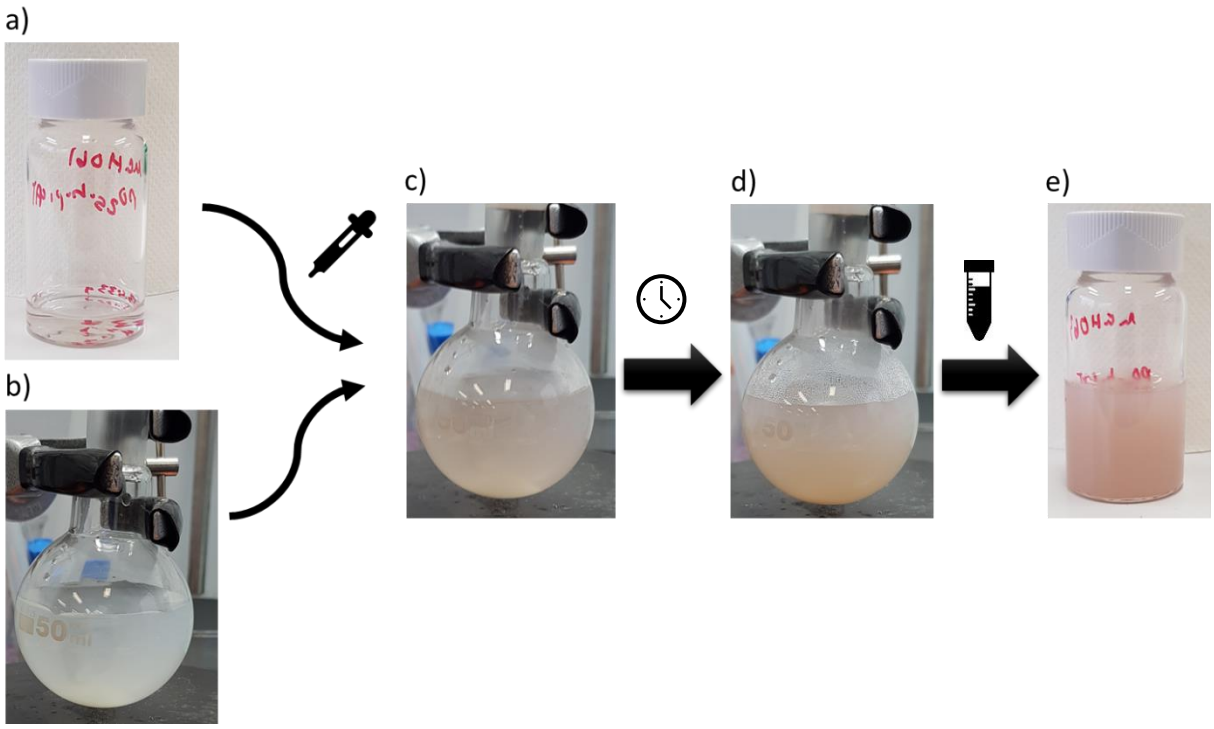

Fig. S19 The procedure of coating NC with P(OEGMA)$_x$-*b*-P(CAT)$_y$: a) P(OEGMA)$_x$-*b*-P(CAT)$_y$ solution in MeOH (15 mg/mL); b) NC dispersion in Milli-Q water (0.5 mg/mL); c) instant colour change in NC dispersion from pale yellow to pale violet upon addition of P(OEGMA)$_x$-*b*-P(CAT)$_y$; d) the pale violet colour became darker overnight; e) purified P(OEGMA)$_x$-*b*-P(CAT)$_y$-NC redispersed in Milli-Q water (1.1 mg/mL).

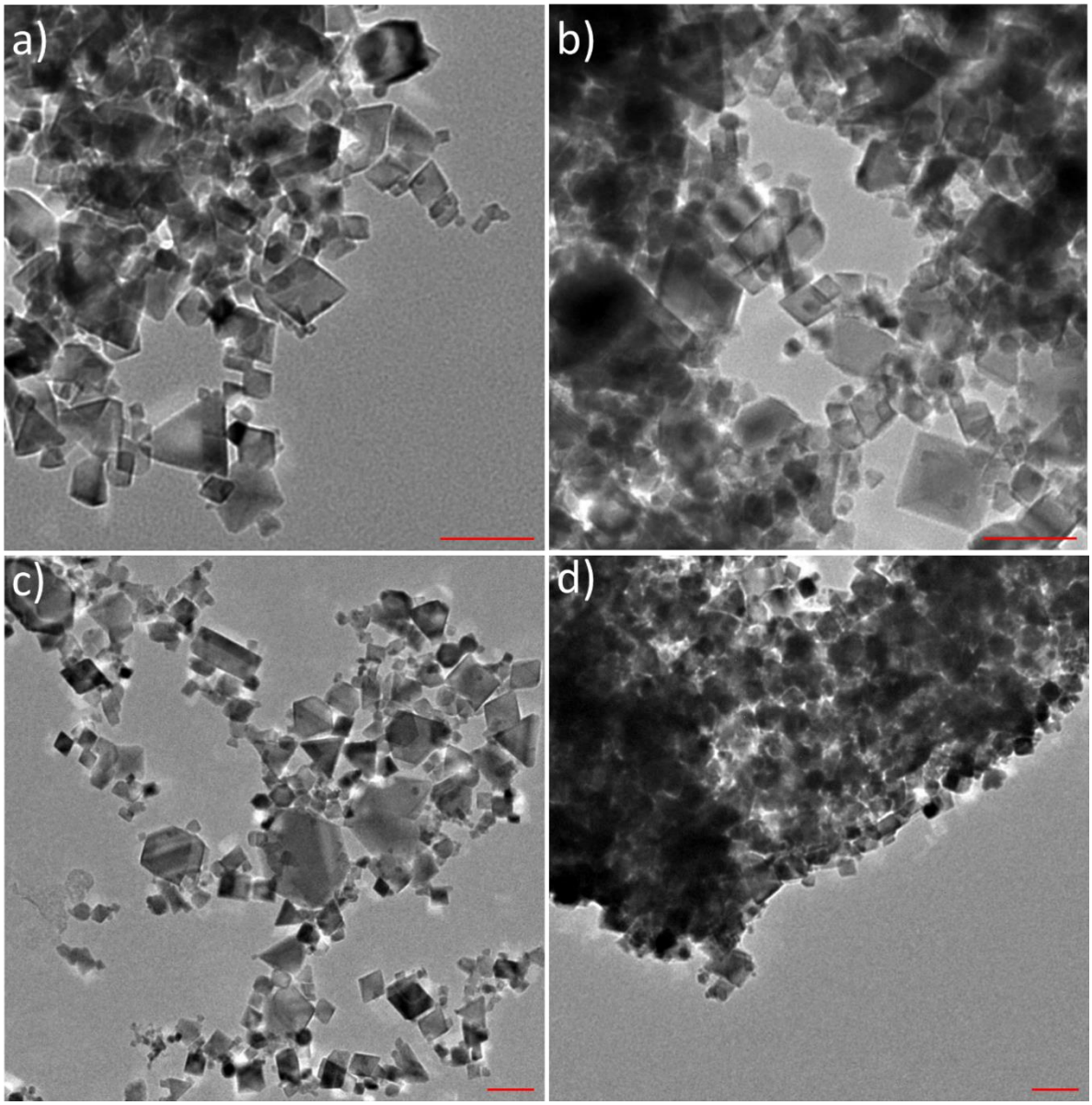

Fig. S20 TEM images of a) bare NC, b) P(OEGMA)$_{25}$-*b*-P(CAT)$_{7}$-NC, c) P(OEGMA)$_{55}$-*b*-P(CAT)$_{4}$-NC, and d) P(OEGMA)$_{55}$-*b*-P(CAT)$_{7}$-NC. Scale bare 50 nm.

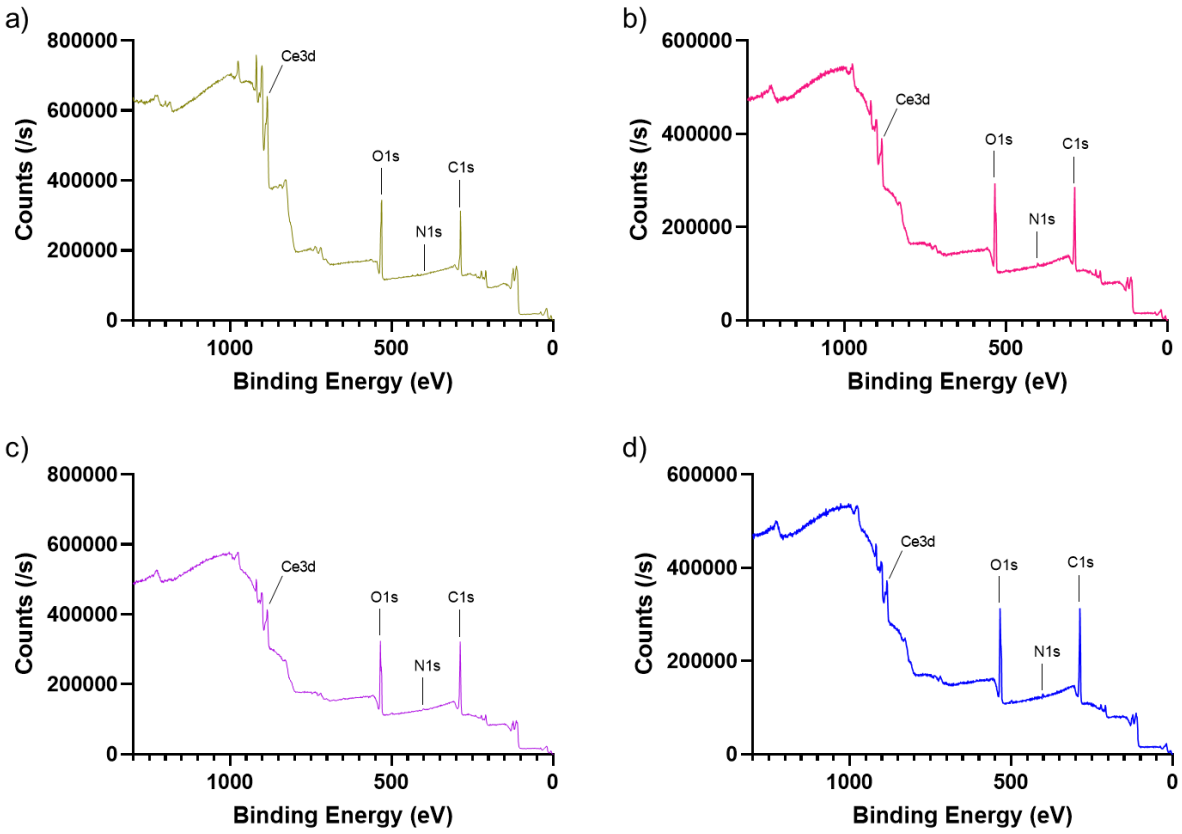

Fig. S21 XPS survey spectra of a) bare NC, b) $P(OEGMA)_{25}$-*b*-$P(CAT)_{7}$-NC, c) $P(OEGMA)_{55}$-*b*-$P(CAT)_{4}$-NC, and d) $P(OEGMA)_{55}$-*b*-$P(CAT)_{7}$-NC.

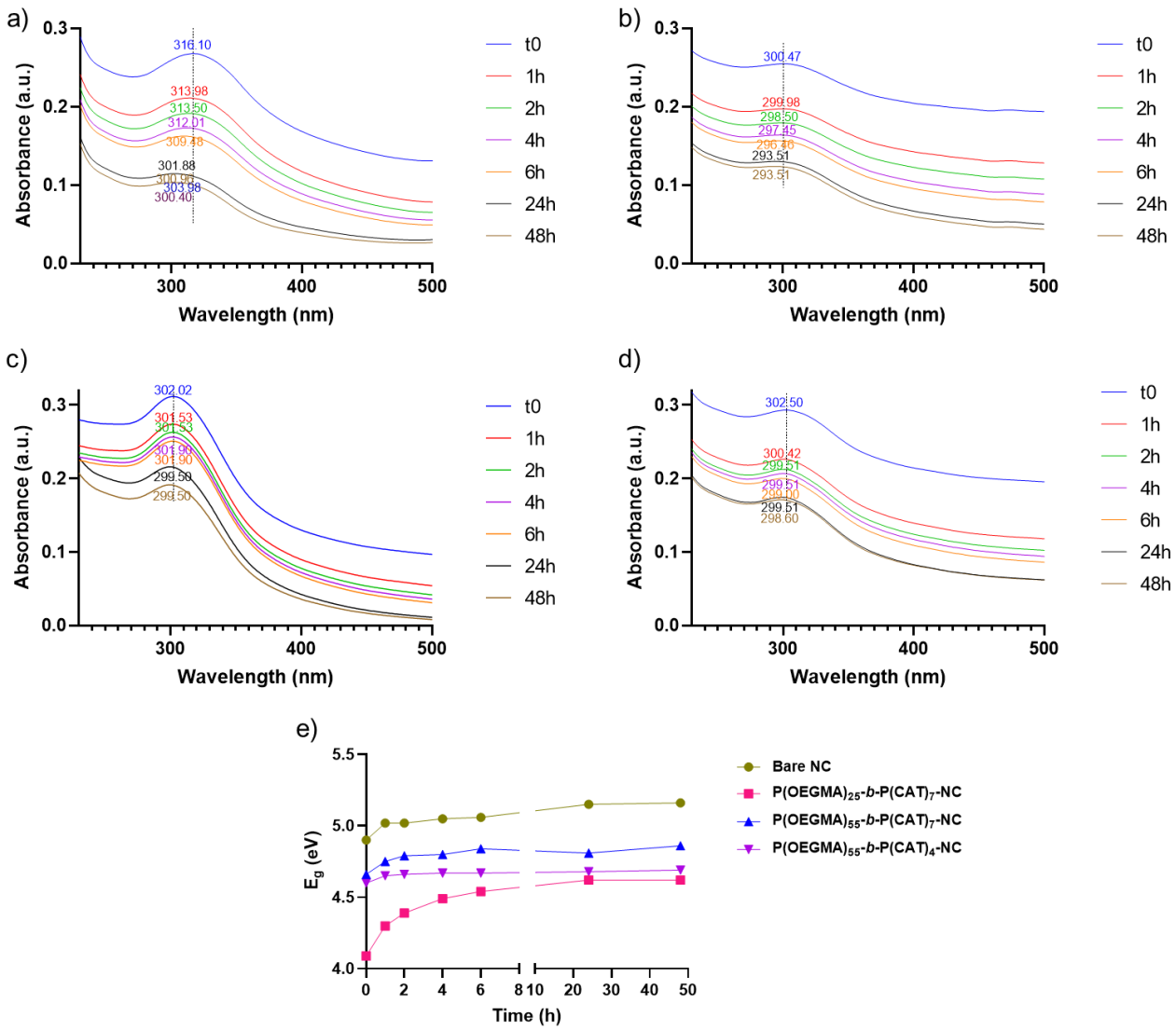

Fig. S22 Colloidal stability analysis for bare and P(OEGMA)$_x$-*b*-P(CAT)$_y$ coated NC samples: the obtained UV-Vis spectra in PBS (1X, pH 7.4) medium at NC concentration of 100 µg/mL over 48 h of analysis for a) bare NC (peaks at 316-300 nm), b) P(OEGMA)$_{25}$-*b*-P(CAT)$_7$-NC (peaks at 300-293 nm), c) P(OEGMA)$_{55}$-*b*-P(CAT)$_4$-NC (peaks at 299-302), and d) P(OEGMA)$_{55}$-*b*-P(CAT)$_7$-NC (298-302 nm). e) The calculated band-gap energy (E_g) via extrapolation of Tauc equation showing an incremental trend over time as a result of the observed blue-shift in the corresponding UV-Vis spectra.

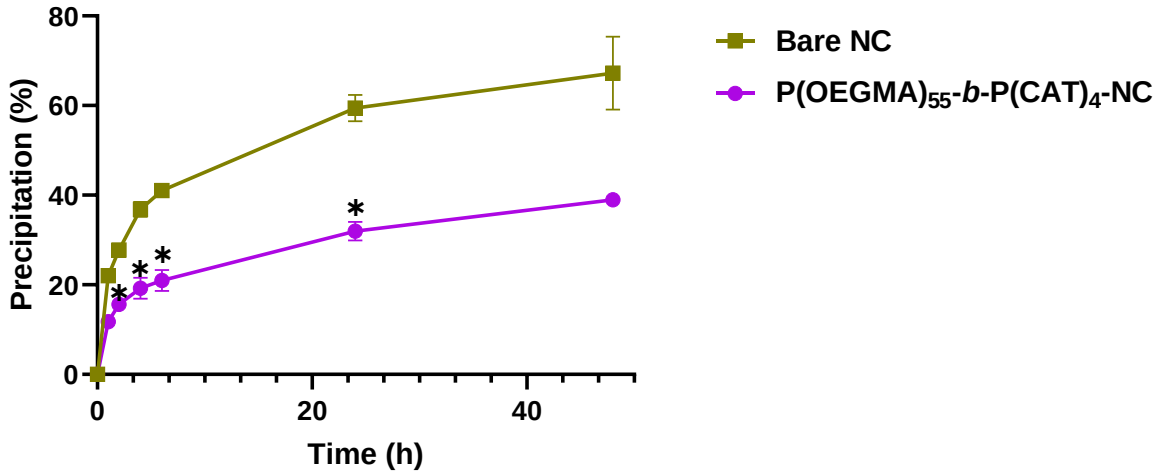

Fig. S23 Colloidal stability analysis for bare and P(OEGMA)$_{55}$-*b*-P(CAT)$_4$ coated NC samples. The results are reported as mean ± SD values (n=2). Statistical significance was calculated via ordinary two-way ANOVA with Dunnett's multiple comparisons post hoc test (GraphPad Prism 9.0.1) with a 95% confidence interval. * P < 0.05.

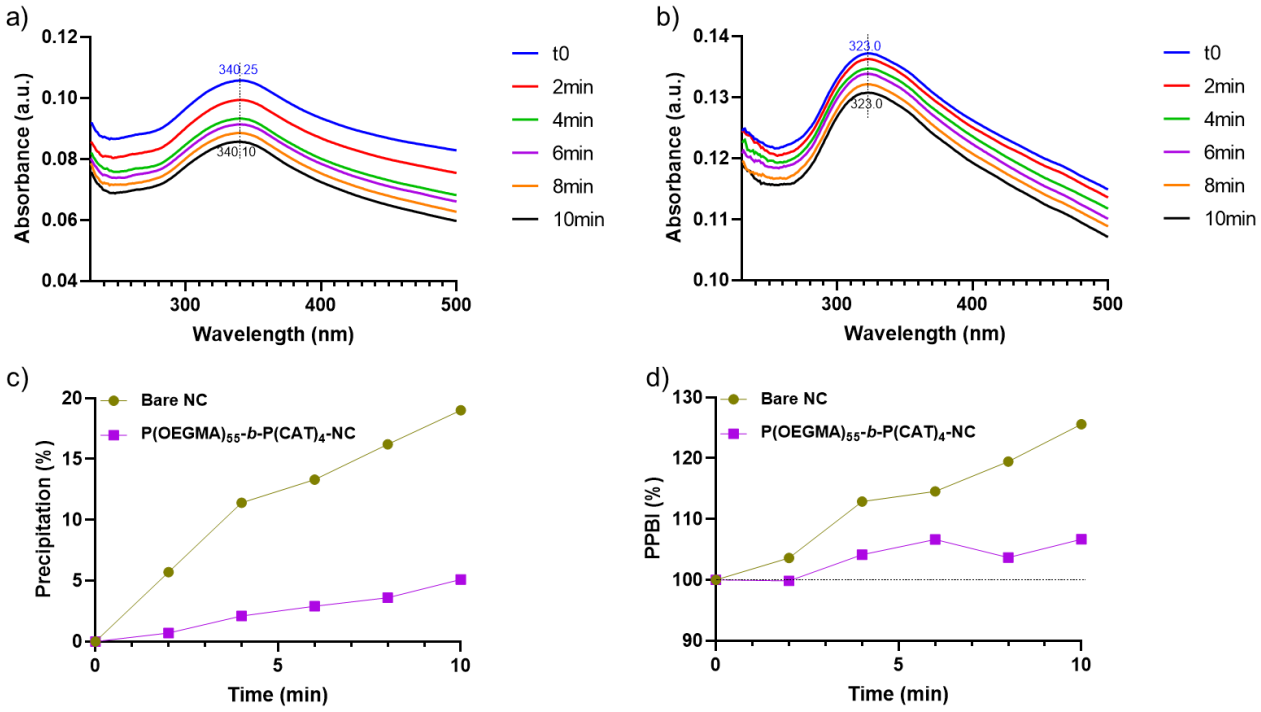

Fig. S24 Colloidal stability analysis for bare and P(OEGMA)$_{55}$-*b*-P(CAT)$_4$ coated NC samples to further investigate the obtained results for SOD-like activity assay: the obtained UV-Vis spectra in PBS (10X, pH 7.4) medium at NC concentration of 100 µg/mL over 10 min of analysis for a) bare NC (peak at around 340 nm) and b) P(OEGMA)$_{25}$-*b*-P(CAT)$_7$-NC (peak at around 323 nm) with no noticeable blue-shift over time. c) The calculated precipitation (%) vs. time showing a noticeable difference between bare NC and P(OEGMA)$_{55}$-*b*-P(CAT)$_4$-NC. d) Plasmon peak broadening index (PPBI) values, indicating polydispersity trends, over 10 min determined based on the full width at half maximum

(FWHM) values of the corresponding UV-Vis spectra calculated via a non-linear curve fitting by the Gaussian function on OriginPro 9.1.

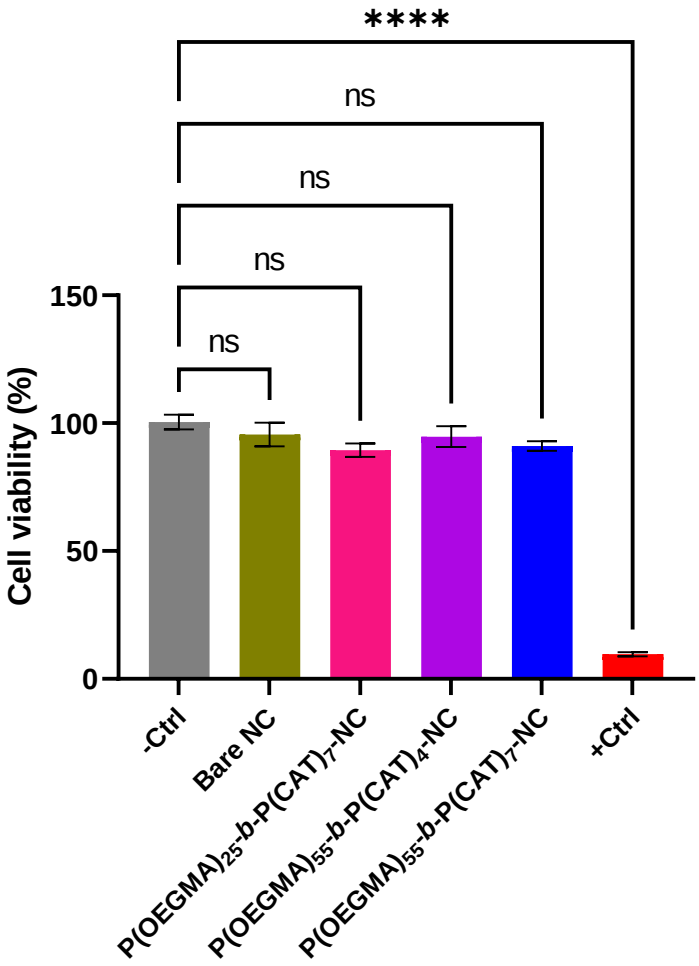

Fig. S25 Cytotoxicity assay for bare and P(OEGMA)$_x$-*b*-P(CAT)$_y$ coated NC samples against Human Embryonic Kidney (HEK) 293 cells at the NC concentration of 100 μg/mL over 24 h. -Ctrl (100% viability): PBS, +Ctrl (<10% viability): 10% (v/v) ethanol 80%. The results are reported as mean ± SEM values (n=3). Statistical significance was calculated via ordinary one-way ANOVA with Dunnett's multiple comparisons post hoc test (GraphPad Prism 9.0.1) with a 95% confidence interval. ns: no significant, **** $P \leq 0.0001$.

References

1. Lyu GM, Wang YJ, Huang X, Zhang HY, Sun LD, Liu YJ, et al. Hydrophilic CeO2 nanocubes protect pancreatic β-cell line INS-1 from H2O2-induced oxidative stress. Nanoscale. 2016;8(15):7923-32.
2. Kwon HJ, Cha MY, Kim D, Kim DK, Soh M, Shin K, et al. Mitochondria-Targeting Ceria Nanoparticles as Antioxidants for Alzheimeŕs Disease. ACS Nano. 2016;10(2):2860-70.
3. Caputo F, Mameli M, Sienkiewicz A, Licoccia S, Stellacci F, Ghibelli L, et al. A novel synthetic approach of cerium oxide nanoparticles with improved biomedical activity. Scientific Reports. 2017;7(1).
4. Grillone A, Li T, Battaglini M, Scarpellini A, Prato M, Takeoka S, et al. Preparation, characterization, and preliminary in vitro testing of nanoceria-loaded liposomes. Nanomaterials. 2017;7(9).
5. Mitra RN, Gao R, Zheng M, Wu MJ, Voinov MA, Smirnov AI, et al. Glycol Chitosan Engineered Autoregenerative Antioxidant Significantly Attenuates Pathological Damages in Models of Age-Related Macular Degeneration. ACS Nano. 2017;11(5):4669-85.
6. Garzón-Manjón A, Aranda-Ramos A, Melara-Benítez B, Bensarghin I, Ros J, Ricart S, et al. Simple Synthesis of Biocompatible Stable CeO2 Nanoparticles as Antioxidant Agents. Bioconjugate Chemistry. 2018;29(7):2325-31.
7. Wang K, Mitra RN, Zheng M, Han Z. Nanoceria-loaded injectable hydrogels for potential age-related macular degeneration treatment. Journal of Biomedical Materials Research - Part A. 2018;106(11):2795-804.
8. Battaglini M, Tapeinos C, Cavaliere I, Marino A, Ancona A, Garino N, et al. Design, Fabrication, and in Vitro Evaluation of Nanoceria-Loaded Nanostructured Lipid Carriers for the Treatment of Neurological Diseases. ACS Biomaterials Science and Engineering. 2019;5(2):670-82.
9. Damle MA, Jakhade AP, Chikate RC. Modulating Pro- A nd Antioxidant Activities of Nanoengineered Cerium Dioxide Nanoparticles against Escherichia coli. ACS Omega. 2019;4(2):3761-71.
10. Hanafy BI, Cave GWV, Barnett Y, Pierscionek B. Ethylene glycol coated nanoceria protects against oxidative stress in human lens epithelium. RSC Advances. 2019;9(29):16596-605.
11. Moleavin IAT, Fifere A, Lungoci AL, Rosca I, Coroaba A, Peptanariu D, et al. In vitro and in vivo antioxidant activity of the new magnetic-cerium oxide nanoconjugates. Nanomaterials. 2019;9(11).
12. Fernández-Varo G, Perramón M, Carvajal S, Oró D, Casals E, Boix L, et al. Bespoken Nanoceria: An Effective Treatment in Experimental Hepatocellular Carcinoma. Hepatology. 2020;72(4):1267-82.
13. Ju X, Fučíková A, Šmíd B, Nováková J, Matolínová I, Matolín V, et al. Colloidal stability and catalytic activity of cerium oxide nanoparticles in cell culture media. RSC Advances. 2020;10(65):39373-84.
14. Pinna A, Cali E, Kerherve G, Galleri G, Maggini M, Innocenzi P, et al. Fulleropyrrolidine-functionalized ceria nanoparticles as a tethered dual nanosystem with improved antioxidant properties. Nanoscale Advances. 2020;2(6):2387-96.
15. Zhao S, Li Y, Liu Q, Li S, Cheng Y, Cheng C, et al. An Orally Administered CeO2@Montmorillonite Nanozyme Targets Inflammation for Inflammatory Bowel Disease Therapy. Advanced Functional Materials. 2020;30(45).
16. Genchi GG, Degl'innocenti A, Martinelli C, Battaglini M, De Pasquale D, Prato M, et al. Cerium Oxide Nanoparticle Administration to Skeletal Muscle Cells under Different Gravity and Radiation Conditions. ACS Applied Materials and Interfaces. 2021;13(34):40200-13.
17. Wu Y, Zhang R, Tran HDN, Kurniawan ND, Moonshi SS, Whittaker AK, et al. Chitosan Nanococktails Containing Both Ceria and Superparamagnetic Iron Oxide Nanoparticles for Reactive Oxygen Species-Related Theranostics. ACS Applied Nano Materials. 2021;4(4):3604-18.
18. Del Turco S, Cappello V, Tapeinos C, Moscardini A, Sabatino L, Battaglini M, et al. Cerium oxide nanoparticles administration during machine perfusion of discarded human livers: A pilot study. Liver Transplantation. 2022;28(7):1173-85.

19. Rai N, Kanagaraj S. Enhanced Antioxidant Ability of PEG-Coated Ce0.5Zr0.5O2-Based Nanofluids for Scavenging Hydroxyl Radicals. ACS Omega. 2022;7(26):22363-76.
20. Yook SH, Kim HY, Kim SJ, Choi S, Kwon T, Cho H, et al. Boosting antioxidation efficiency of nonstoichiometric CeOx nanoparticles via surface passivation toward robust polymer electrolyte membrane fuel cells. Chemical Engineering Journal. 2022;432.
21. Liu D, Lu G, Shi B, Ni H, Wang J, Qiu Y, et al. ROS-Scavenging Hydrogels Synergize with Neural Stem Cells to Enhance Spinal Cord Injury Repair via Regulating Microenvironment and Facilitating Nerve Regeneration. Advanced Healthcare Materials. 2023.
22. Qiao Y, Li J, Bian S, Zhan C, Luo J, Jiang L, et al. Application of biocompatible custom ceria nanoparticles in improving the quality of liver grafts for transplantation. Nano Research. 2023;16(4):5176-88.
23. Zhang Y, Liu S, Peng J, Cheng S, Zhang Q, Zhang N, et al. Biomimetic Nanozymes Suppressed Ferroptosis to Ameliorate Doxorubicin-Induced Cardiotoxicity via Synergetic Effect of Antioxidant Stress and GPX4 Restoration. Nutrients. 2023;15(5).